

Evaluating the performance of quantum process units at large width and depth

J. A. Montañez-Barrera,^{1,*} Kristel Michielsen,^{1,2,3} and David E. Bernal Neira⁴

¹*Jülich Supercomputing Centre, Institute for Advanced Simulation,
Forschungszentrum Jülich, 52425 Jülich, Germany*

²*AIDAS, 52425 Jülich, Germany*

³*RWTH Aachen University, 52056 Aachen, Germany*

⁴*Davidson School of Chemical Engineering, Purdue University, 47907, West Lafayette, Indiana, USA*

Currently, we are in a stage where quantum computers surpass the size that can be simulated exactly on classical computers, and noise is the central issue in extracting their full potential. Effective ways to characterize and measure their progress for practical applications are needed. In this work, we use the linear ramp quantum approximate optimization algorithm (LR-QAOA) protocol [1], a fixed quantum approximate optimization algorithm (QAOA) protocol, as an easy-to-implement scalable benchmarking methodology that assesses quantum process units (QPUs) at different widths (number of qubits) and 2-qubit gate depths. The benchmarking identifies the depth at which a fully mixed state is reached, and therefore, the results cannot be distinguished from those of a random sampler. We test this methodology using three graph topologies: 1D-chain, native layout, and fully connected graphs, on 19 different QPUs from 5 vendors: IBM, IQM, IonQ, Quantinuum, and Rigetti for problem sizes requiring from $N_q = 5$ to $N_q = 156$ qubits and LR-QAOA number of layers from $p = 3$ to $p = 10,000$. In the case of 1D-chain and native graphs, `ibm_fez`, the system with the largest number of qubits, performs best at $p = 15$ for problems involving $N_q = 100$ and $N_q = 156$ qubits and 1,485 and 2,640 2-qubit gates, respectively. For the native graph problem, `ibm_fez` still retains some coherent information at $p = 200$ involving 35,200 fractional 2-qubit gates. Our largest implementation is a 1D-chain problem with $p = 10,000$ involving 990,000 2-qubit gates on `ibm_fez`. For fully connected graph problems, `quantinuum_H2-1` shows the best performance, passing the test with $N_q = 56$ qubits at $p = 3$ involving 4,620 2-qubit gates with the largest 2-qubit gate implementation for a problem with $N_q = 50$ qubits and $p = 10$ involving 12,250 2-qubit gates but not passing the test.

Keywords: Quantum Benchmarking, IBM Heron, IBM Eagle, IQM Garnet, Quantinuum H2-1, Rigetti Ankaa-2, IonQ Aria, Forte, LR-QAOA, Weighted MaxCut.

I. INTRODUCTION

In the current stage of quantum technology, benchmarks are tools that track the evolution of quantum technology to do useful computations. Successful benchmarks have a clear set of rules, are easy to implement, are platform agnostic, and have meaningful metrics associated with performance. One example of a successful benchmark is the quantum volume (QV) [2]. QV expresses the largest square circuit that can be run reliably on a Quantum Processing Unit (QPU). QV is used by different companies [3–6] with the largest value to date coming from `quantinuum_H2-1` with a QV of 2^{21} [7]. It is still a near-term benchmark (< 50 qubits) as the quantum circuits must be simulated classically, and such simulations need exponential resources.

Another successful benchmarking protocol is randomized benchmarking (RB) [8]. Contrary to QV, RB does not give a holistic view of the quality of a QPU but tests the performance of quantum operations. It has the desired property of being easy to implement and scalable, addressing gate errors from a decaying rate

curve. Alternative holistic benchmarks are direct randomized benchmarking (DRB) [9], Mirror randomized benchmarking (MRB) [10], cross-entropy benchmarking (XEB)[11], algorithmic qubits (AQ)[12], error per layered gate (EPLG)[13], or application-oriented performance benchmarks [14–16].

IBM has recently transitioned its primary benchmarking metric from QV to EPLG. EPLG is a scalable benchmarking that leverages randomized benchmarking (RB) on disjoint sets of 2-qubit subsystems. This approach offers the benefit of providing localized error information within subsystems, which can be used to estimate the overall device error. As pointed out in [17, 18], different candidate benchmarks to capture essential aspects of performance should be proposed, and the best of them with the most explicit set of rules and utility will remain.

In this paper, we propose a volumetric benchmark [17] using LR-QAOA to solve a combinatorial optimization problem (COP) with increasing circuit width and depth defined over three types of graphs: 1D-chain, native layout (NL), and fully connected (FC). This protocol increases the correlation between the qubits as the circuit's depth, proportional to the number of layers in QAOA p , grows. The behavior can be characterized by the approximation ratio, r , the ratio between the average over the obtained solutions and the known best possible solution. This metric related to the algorithm's performance satu-

* Corresponding author: J. A. Montañez-Barrera; j.montanez-barrera@fz-juelich.de

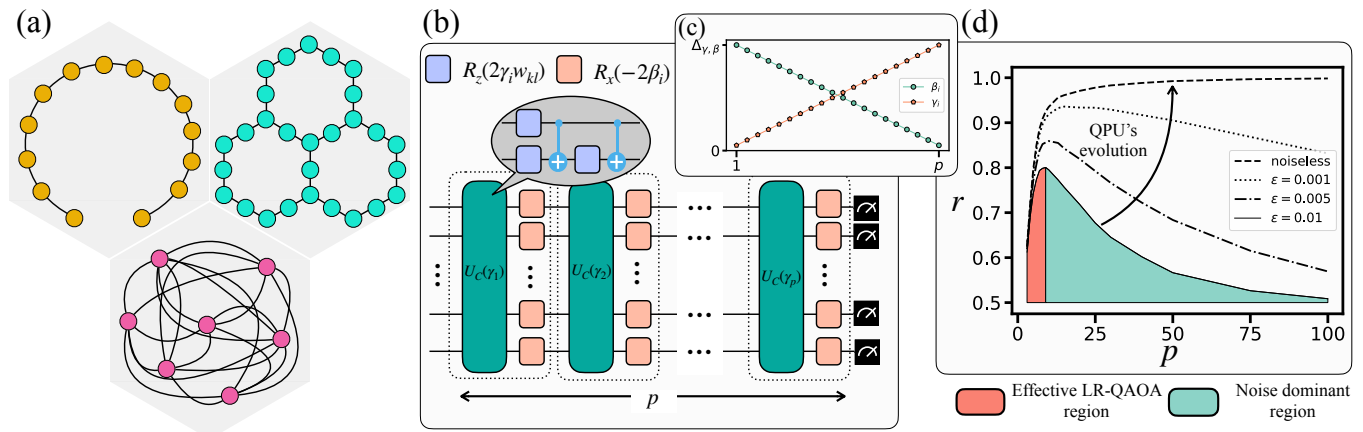


FIG. 1. Scheme of the Quantum Processing Units (QPUs) benchmarking. (a) Graphs used for the benchmarking. In yellow is the 1D-Chain, in green is the native layout (NL), and in pink is the fully connected (FC) graph. (b) QAOA protocol consists of alternating layers of the problem Hamiltonian and the mixer Hamiltonian. p represents the depth of the algorithm. (c) Schedule of the LR-QAOA algorithm, $\Delta_{\gamma,\beta}/p$ is the slope. (d) Expected results of LR-QAOA in terms of approximation ratio versus number of LR-QAOA layers. Black curves represent different levels of depolarizing noise strength.

rates at $r = 1$ for large depth p . These benchmarks are scalable, easy to implement, and give valuable information on the holistic QPU performance.

In Fig. 1, we show the LR-QAOA benchmarking schemes. Fig. 1-(a) shows the three types of graphs analyzed. The first two benchmarks, 1D-chain and NL, are thought for fixed layout devices, e.g., IBM Heavy-Hex lattice [19], while the FC benchmark is considered for both fixed-layout and FC QPU, e.g., `quantinuum_H2-1`.

Figure 1(b) shows the QAOA circuit used for the protocol. QAOA [20] aims to find low-energy solutions of a Hamiltonian that represents a given COP. It consists of p alternating layers of parametric gates representing a problem Hamiltonian and a mixer Hamiltonian. In this work, the problem Hamiltonian is encoded in the unitary operation U_C , corresponding to a weighted maxcut problem (WMC). The WMC problem aims to partition the nodes in a weighted graph into two groups so that the sum of the weights of the edges going across the partition is maximized. This problem is NP-Hard [21], meaning that there is no deterministic polynomial-time algorithm to solve it unless $P=NP$, and it is equivalent to finding the ground state of an Ising spin glass model defined over an equivalent graph [22].

When combined with the parameters of Fig. 1(c), the QAOA protocol resembles a trotterized approximation of the adiabatic algorithm which we denoted as LR-QAOA. The WMC LR-QAOA is suitable for benchmarking quantum technology because it has the desired properties that as p grows, r grows independently of the problem size or graph's shape and can be tailored to any QPU layout.

Figure 1(d) shows the usual LR-QAOA behavior of r versus p for different levels of depolarizing noise ϵ . We can divide the LR-QAOA evolution into the red region, which represents where LR-QAOA dominates the evolution, and the green region, where noise dominates. As

generations of QPUs improve, reducing the noise, we expect the behavior following the arrow in Fig. 1(d).

We showcase the LR-QAOA benchmarking protocol assessing 19 QPUs from 5 vendors: 8 IBM Eagle, 3 IBM Heron, 2 IQM, 2 Quantinuum H, 3 IonQ, and 1 Rigetti. We test LR-QAOA from $p = 3$ up to $p = 10,000$ for the three graph strategies. We observed an evolution of the QPUs' performance within generations of QPUs, e.g., IBM Eagle to IBM Heron or IonQ Harmony to Aria.

The paper is organized as follows. Section II describes LR-QAOA and the experimental setup. In Sec. III, the results of the 1D-Chain, NL, and FC graphs are presented. Finally, Sec. IV provides some conclusions.

II. METHODS

In this section, we present the linear-ramp quantum approximation optimization algorithm (LR-QAOA) and the experimental setup used in the various quantum computational hardware evaluated in this manuscript.

A. LR-QAOA

LR-QAOA is a non-variational version of QAOA [20] that uses linear annealing schedules for the parameters of QAOA (Fig. 1(c)). It can be seen as a first-order trotterized approximation of an adiabatic quantum evolution [23]. It consists of alternating layers of unitary gates that describe a problem Hamiltonian with an unknown ground state along with a mixer Hamiltonian whose ground state is prepared at the beginning of the evolution. In quantum optimization, the problem Hamiltonian usually represents a COP. As the system evolves, the average energy decreases, amplifying good solutions for the COP. In our

case, we choose WMC because it can be adapted to any graph, and its Hamiltonian involves only 2-qubit interactions. In Sec. A 1, we present a description of WMC. The WMC cost Hamiltonian is given by

$$H_C = \sum_{\{i,j\} \in E(\mathcal{G})} w_{ij} \sigma_z^i \sigma_z^j, \quad (1)$$

where σ_z^i is the Pauli-z term of qubit i . The WMC is defined over a weighted graph \mathcal{G} where w_{ij} is the weight associated with the edge between vertices i and j . For LR-QAOA, qubit i is a representation of a vertex of \mathcal{G} , $V(\mathcal{G})$. H_C is encoded into a parametric unitary gate given by

$$U_C(H_C, \gamma_k) = e^{-j\gamma_k H_C}, \quad (2)$$

where γ_k is a parameter that comes from the linear ramp schedule and $j = \sqrt{-1}$. Following this, in every second part of a layer, the mixer unitary operator is applied given by

$$U(H_B, \beta_i) = e^{j\beta_i H_B}, \quad (3)$$

where β_i is taken from the linear ramp schedule and $H_B = \sum_{i=0}^{N_q-1} \sigma_i^x$ with σ_i^x the Pauli-x term of qubit i . The general QAOA circuit is shown in Fig. 1-(b). Here, $R_X(-2\beta_i) = e^{j\beta_i \sigma_i^x}$, p is the number of repetitions of the unitary gates of Eqs. 2 and 3, and the initial state is a superposition state $|+\rangle^{\otimes N_q}$. Repeated preparation and measurement of the final LR-QAOA state yields a set of candidate solution samples, improving their quality as p grows.

In Fig 1(c), we show the LR-QAOA protocol. It is characterized by three parameters: Δ_β , Δ_γ , and the number of layers p . The β_i and γ_i parameters are given by

$$\beta_i = \left(1 - \frac{i}{p}\right) \Delta_\beta \quad \text{and} \quad \gamma_i = \frac{i+1}{p} \Delta_\gamma, \quad (4)$$

for $i = 0, \dots, p-1$. For our simulations and experimental results, we use $\Delta_\beta = \Delta_\gamma = \Delta_{\beta,\gamma}$. $\Delta_{\beta,\gamma}$ values for the different experiments are summarized in Sec. A 3.

B. Experimental Setup

Table I summarizes the number of qubits N_q , the 2-qubit gate time, the 2-qubit gate error, and the layout connectivity of some QPUs used in this work. The information about IBM devices comes from [24], `ionq_aria_2` and `ionq_harmony` from [25], information about `quantinuum_H1-1` [26] and `quantinuum_H2-1` [27], `iqm_garnet` from [6], and `rigetti_ankaa_2` from [28]. We could not find information about the 2-qubit gate time from `quantinuum_H1-1` and `quantinuum_H2-1`.

Implementing p layers of LR-QAOA for the 1D-chain cases using IBM, Rigetti, and IQM QPUs requires $N_{2q} =$

TABLE I. QPU's number of qubits (N_q), two-qubit native gate time (t_{2q}), average two-qubit error (ϵ_{2q}), and native layout (NL) with heavy-Hex (HE), square (SQ), or fully connected (FC).

QPU	Properties			
	N_q	t_{2q}	ϵ_{2q}	NL
<code>ibm_brisbane</code>	127	600 ns	7.760e-3	HE
<code>ibm_torino-v1</code>	133	68/184 ns	2.977e-3	HE
<code>ibm_fez</code>	156	68 ns	2.959e-3	HE
<code>ibm_marrakesh</code>	156	68 ns	2.157e-3	HE
<code>quantinuum_H1-1</code>	20	-	0.860e-3	FC
<code>quantinuum_H2-1</code>	56	-	1.300e-3	FC
<code>ionq_forte</code>	36	970 μ s	4.000e-3	FC
<code>ionq_aria_2</code>	25	600 μ s	4.000e-3	FC
<code>ionq_harmony</code>	11	210 μ s	39.80e-3	FC
<code>iqm_spark</code>	5	≤ 100 ns	10.00e-3	SQ
<code>iqm_garnet</code>	20	20/40 ns	5.000e-3	SQ
<code>rigetti_ankaa_2</code>	84	68 ns	55.60e-3	SQ

$2p(N_q - 1)$ two-qubit CZ gates while the depth grows as $d = 4p$. In the case of the NL, the number of 2-qubit gates varies depending on the device but the depth is given by $d = 6p$ on IBM QPUs while $d = 8p$ on IQM QPUs. The FC case following the methodology presented in Sec. A 7 requires $N_{2q} = 3pN_q(N_q - 1)/2$ 2-qubit CZ gates for fixed-layout QPUs and $N_{2q} = pN_q(N_q - 1)/2$ for `quantinuum_H2-1` with $d = 3pN_q$ on fixed-layout QPUs and $d = pN_q(N_q - 1)/8$ on `quantinuum_H2-1`. We use 1,000 samples in experiments on IBM, IQM, and Rigetti QPUs, 100 samples on IonQ, 50 samples on `quantinuum_H2-1` with $N_q \leq 50$, and seven samples for $N_q = 56$.

Recently, IBM introduced fractional gates [29] on Heron devices which directly implement the ZZ and rx gates needed for LR-QAOA. In the case of 1D-chain and NL problems, this reduces the number of 2-qubit gates and the 2-qubit depth to half of that needed when using CZ gates.

III. RESULTS

The results of the 1D-chain experiments are designed to provide a meaningful diagnostic of the qubit performance in the longest available qubit-chain of a QPU. This information is meaningful because this chain is used afterward for the FC problems using the SWAP strategy discussed in Sec. A 7. Fig. 2(a) shows the r versus the number of LR-QAOA layers for a WMC with 100 qubits on different IBM QPUs which requires $N_{2q} = 19,800$ to implement the $p=100$ case. Some QPU results are summarized in Table II with an improved performance seen on the newer Heron family of QPUs `ibm_marrakesh`, `ibm_fez`, and `ibm_torino-v1` (post firmware update of `ibm_torino-v0`). In contrast, older devices from the Eagle family show comparatively lower performance, with the best result com-

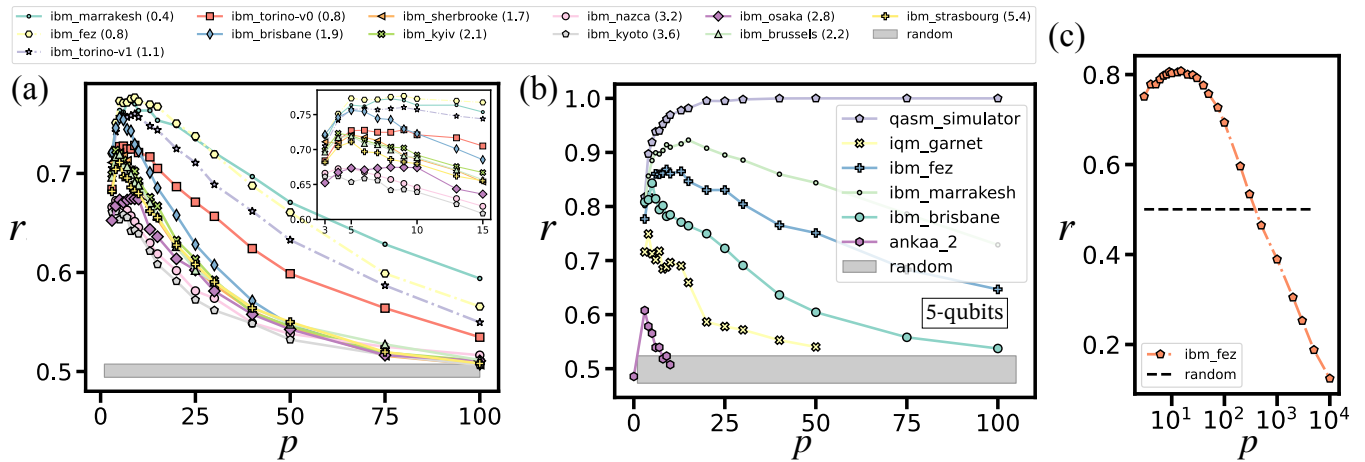


FIG. 2. Approximation ratio versus the number of LR-QAOA layers for a 1D-chain WMC with $p=3$ to 100 on IBM, IQM, and Rigetti devices. (a) 100 qubit problem running on different IBM Eagle and Heron devices. The values in parenthesis above the plots are the EPLG at the moment of the experiment. (b) Multiplatform benchmarking comparison for a 5-qubit problem on IBM Eagle, Heron, IQM garnet, and Rigetti Ankaa. (c) *ibm_fez* 100 qubit experiment for $p=3$ to $p=10,000$ using fractional gates involving 990,000 ZZ gates for the $p=10,000$ experiment.

ing from *ibm_brisbane*. The remaining devices can be grouped into two clusters based on similar performance levels: the first group includes *ibm_sherbrooke*, *ibm_kyiv*, *ibm_brussels*, and *ibm_strasbourg*, while the second group consists of *ibm_nazca*, *ibm_kyoto*, and *ibm_osaka*. Note that the EPLG does not necessarily agree with the performance of the device; for instance, *ibm_torino-v1* has an EPLG=1.1 while *ibm_torino-v0* EPLG=0.8, but the approximation ratio of *ibm_torino-v1* is larger than that of *ibm_torino-v0*. In Sec. A 5, we present additional experiments that show that there is only a small variation in the approximation ratio if the total number of qubits varies from 30 to 100 qubits, Fig. 8(d) or if the experiment is repeated in different days spanned during 2 months Fig.8(e).

Figure 2(b) shows the approximation ratio versus the number of LR-QAOA layers for various IBM QPUs, IQM Garnet, and Rigetti Ankaa for a 5-qubit WMC problem. A good first indication of the performance of the QPU comes from the 2-qubit error in Table I. For instance, Rigetti Ankaa has an order of magnitude larger error than IQM Garnet, and the approximation ratio of LR-QAOA captures the low performance in Rigetti Ankaa. However, other factors, such as crosstalk, are not captured by the 2-qubit error and can be exposed by this benchmark; for instance, *ibm_brisbane* has a larger 2-qubit error than *iqm_garnet* but still shows better performance, it might indicate that *ibm_brisbane* deal better with errors coming from other sources. The improvement from *ibm_brisbane* to *ibm_fez* is seen in terms of the maximum approximation ratio and the decaying rate.

Figure 2(c) shows the 1D-chain implementation of the 100 qubit experiment using fractional gates on *ibm_fez*. An interesting phenomenon that will repeat using NL problems is a relaxation that destroys any improvement

gained using LR-QAOA after $p = 300$. In the limit of $p = 10,000$, the device does not act even as a random sampler instead many of the qubits are already back in $|0\rangle$. This experiment is our largest implementation involving almost a million 2-qubit gates and shows that even if it does not produce meaningful information at least it can be executed. The QPU time committed to obtain 1,000 samples running the $p = 10,000$ LR-QAOA circuit is 21 seconds.

The holistic evaluation of the 1D-chain test is also evident in the *ibm_marrakesh* experiments. Despite this device having the lowest (EPLG=0.4%), its performance does not exceed that of the *ibm_fez* (EPLG=0.8%) when scaling up to the 100-qubit case. On the other hand, when the number of qubits is low, such as in the 5-qubit case, the EPLG metric certainly aligns with the observed performance. It might indicate that at a large number of qubits, there are other factors not fully captured by the EPLG metric.

Figure 3 presents the solutions to problems involving the full set of qubits and 2-qubit gates for different QPUs. In Fig. 3(a), the layouts of the QPUs, including *iqm_spark*, *iqm_garnet*, IBM Eagle, and two versions of IBM Heron, r1 $N_q = 133$ qubits and r2 $N_q = 156$ qubits, are presented. The edges in Fig. 3(a) show the random values for the WMC problem chosen from the set $\{0.1, 0.2, 0.03, 0.5, 1\}$ in each NL problem. These tests help understand the performance of QPUs working as a whole.

Figure 3(b) shows the approximation ratio versus p for devices with different NL. The maximum approximation ratio for the QPUs is summarized in Table II. *ibm_fez* has the largest number of qubits and 2-qubit gates involved in the experiment that, in principle, can reduce its performance; this is not the case, and this

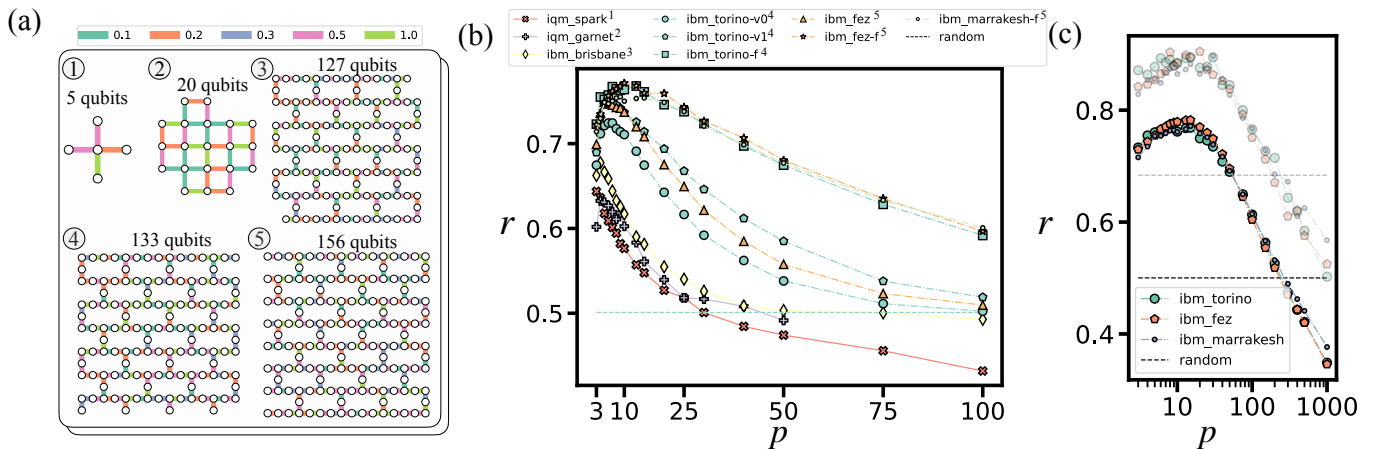


FIG. 3. NL-based benchmarking using LR-QAOA for WMC problems with 5 (4), 20 (30), 127 (144), 133 (150), and 156 (176) qubits (edges) on *iqm_spark*, *iqm_garnet*, *ibm_brisbane*, *ibm_torino*, and *ibm_fez/ibm_marrakesh*, respectively. (a) Layout of the QPUs the nodes represent the qubits and the edges are the physical connection for 2-qubit operations. Colors represent the random weights for the WMC with the possible values shown in the upper part of the figure. (b) Shows the approximation ratio versus LR-QAOA layers of the WMC for different processors. The dashed line in these plots represents the random limit. The f after the name, e.g. *ibm_marrakesh-f*, means that fractional gates are used in the experiment. (c) Experiment using fractional gates and up to $p=1000$ LR-QAOA layers. The semitransparent points indicate the sample with the maximum approximation ratio found.

QPU shows the best performance. This might indicate that the quality of its qubits to work altogether is superior to the other QPUs. To implement the largest case ($p=100$) on each device shown is $N_{2q} = 105,600$ on *ibm_fez*, $N_{2q} = 90,000$ on *ibm_torino*, $N_{2q} = 86,400$ on *ibm_brisbane*, $N_{2q} = 12,000$ on *iqm_garnet*, and $N_{2q} = 3,200$ on *iqm_spark*. For the case of fractional gates, the number of 2-qubit gates is reduced to half, therefore, to implement the same methodology on *ibm_fez* it is needed only $N_{2q} = 45,000$ for $p=100$. These experiments offer a perspective on QPU evolution, such as the progression from IBM’s Eagle to Heron architectures that can be used as a baseline for future QPUs.

There is no direct comparison between different QPUs due to variations in problem sizes and connectivity. However, the NL curves exhibit similar growth and saturation patterns that might be used as an indicator of the average qubit quality. IBM’s Heron devices show the best performance with *ibm_fez* $r_{max} = 0.750$ followed by *ibm_torino-v1* $r_{max} = 0.746$. These results agree with the 1D-chain (see Fig. 2(b)), but in this case, the decaying rate of the approximation ratio is slower in the *ibm_torino-v1* case. At $p = 30$, the approximation ratio in *iqm_spark* shows a performance below the random sampler limit, which means that the probability distribution is biased by a distribution that is not random nor guided by LR-QAOA, which can be a consequence of thermalization phenomena on the QPU. In Sec. A 6, an extended explanation of the NL tests is presented.

Fig. 3(c) shows the largest NL implementation in terms of p layers, reaching the $p = 1,000$ limit. This corresponds to 176,000 2-qubit ZZ gates in the *ibm_fez/ibm_marrakesh* experiments. For the devices,

$p = 200$ is the limit where still some coherent information of the optimization is present, this corresponds to 35,200 ZZ gates and a 2-qubit depth of 600 which requires a time of $40.8\mu s$. Interestingly, the thermalization phenomenon observed from $p > 30$ in *iqm_spark* is observed at $p > 200$ in IBM Heron QPUs.

Figure 4 shows the results for the FC test on QPUs from different vendors. This test involves $N_{ZZ} = pN_q(N_q - 1)/2$ two-qubit ZZ gates. In the case, of the largest successful experiment, H2-1 $N_q = 56$, the number of layers implemented is $p = 3$ and the gates used are $N_{2q} = N_{ZZ} = 4,620$. In the case of IBM QPUs, the best result comes from *ibm_fez* passing the test with $p = 3$ for $N_q = 20$. This test on fixed 1D-chain layout requires $N_{2q} = 3N_{ZZ}$ using the SWAP network strategy (See Sec.A 7), this means $N_{2q} = 1,710$ CZ gates. In the case of IonQ Aria 1 and IonQ Forte, there is a restriction $N_{2q} = N_{ZZ} < 650$ operations in the circuit. Therefore, results are only presented up to 21 qubits where the restriction is still satisfied by LR-QAOA $p = 3$. It is still highly possible to get successful results if the N_{2q} increases using these devices.

Figure 4-(a) shows the experiment of $N_q = 15$ and $p = 0$ to $p = 50$. We include $p = 0$ to show the behavior of only applying the Hadamard gates. As we show with the *qasm_simulator*, at $p = 0$ the result falls in the region of a random sampler, the behavior expected by creating a superposition state with the Hadamard gates. In the ideal case (*qasm_simulator*), r grows monotonically and saturates at $r = 1$. The emulator H1-1E, which closely represents the noise in the real device *quantinuum_H1-1*, maintains a close performance to *qasm_simulator* for $p < 10$, and then its noise does not fully compensate the

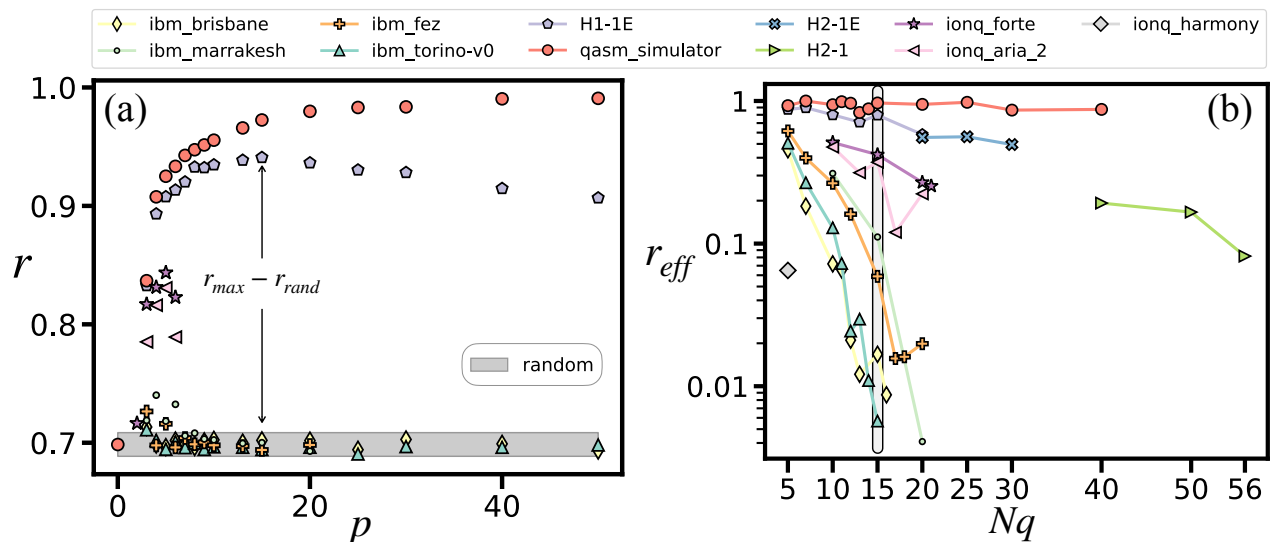


FIG. 4. FC graph benchmarking using LR-QAOA for WMC problems ranging from 5 to 56 qubits. (a) Approximation ratio versus the number of LR-QAOA layers for the 15-qubit WMC problem. (b) Effective approximation ratio versus the number of qubits using different QPUs.

LR-QAOA improvement. The maximum approximation ratio in this case is reached at $r_{max}(p = 15) = 0.94$ and therefore $p_{eff} = 15$. IonQ Aria and Forte pass the test with the peaking performance at $r_{max}(p = 5) = 0.83$. IBM QPUs pass the test with the best performance from `ibm_marrakesh`, $r_{max}(p = 4) = 0.740$. The random region of this plot, discussed in detail in Sec. A 2, helps distinguish whether a QPU produces coherent results—indicated by an approximation ratio above the random region—or whether it reaches a fully mixed state, falling within the random region.

Figure 4(b) shows r_{eff} (Eq. A4) for different QPUs and problem sizes. This plot summarizes the experiments like the one shown in Fig. 4(a) for different numbers of qubits. From each experiment, the best solution is taken if it does not fall in the random region. Therefore, every point shown is above a 99.73% confidence interval of a random sampler mean approximation ratio (See Sec. A 2). Results on IBM QPUs show progress from the Eagle to the Heron r1 to Heron r2 generations. For instance, `ibm_brisbane` (Eagle) and `ibm_torino-v0` (Heron r1) only pass the test with 16 and 15 qubits, respectively. On the other hand, `ibm_fez` (Heron r2) passes the test up to 20 qubits. It means a 58% improvement in the number of 2-qubit gates that maintain some coherent information from $N_{2q} = 1,080$ to $N_{2q} = 1,710$. In the case of `ibm_marrakesh`, we observed the same characteristics of the 1D-Chain and NL experiments. For small cases, $N_q \leq 15$, `ibm_marrakesh` outperforms `ibm_fez`, but when the problem size grows above that limit, `ibm_fez` has a better performance.

We test the implementation limits and find that we can encode a 100-qubit FC problem with $p = 20$ involving $N_{2q} = 297,000$, and even though the results cannot be

distinguished from those of a random sampler, it means that IBM QPUs are prepared to run long circuits. In the case of `quantinuum_H2-1`, we try to run a 50-qubit problem with $p = 15$, which requires $N_{2q} = 18,375$. However, the circuit size exceeds the maximum allowed. A summary of the FC results on different QPUs is shown in Table II for 20-qubit and the largest implementation on different QPUs. Additional details about the correlation generated during the LR-QAOA evolution are presented in Sec. A 8.

The quality of the solutions in the case of `ionq_aria_2` is better than that of IBM but no points after 20 qubits are presented because of the limitation of a maximum of $N_{2q} < 650$. The strength of `ionq_aria_2` lies in its fully connected (FC) architecture, allowing it to implement the 20-qubit case with only $N_{2q} = 190p$, whereas IBM QPUs require $N_{2q} = 570p$ (three times more gates). However, its weakness is the slower gate speed (600 μ s) and the fact that gates are executed sequentially, resulting in significantly longer implementation times compared to superconducting technology (See Sec. A 9). In the case of `ionq_forte`, the latest generation of IonQ’s QPU, there is no noticeable improvement in quality from the results observed in `ionq_aria_2`.

In the case of `quantinuum_H2-1`, the experiments of 50 and 56 qubits are already above the capabilities of exact simulation in HPC systems ($N_q < 50$) [30], and the results are still meaningful. This means that the LR-QAOA protocol maintains some coherent information with protocols involving $N_{2q} = 4,900$ (50 qubits and $p = 4$) and $N_{2q} = 4,620$ (56 qubits and $p = 3$), respectively. To the best of our knowledge, this is the largest implementation of QAOA to solve an FC combinatorial optimization problem on real quantum hardware that is

certified to give a better result over random guessing.

TABLE II. QPU maximum approximation ratio for the different benchmarking graphs. The two values at 1D-chain represent the 5/100 qubit case. The f before the number means that the protocol is executed using fractional gates.

QPU	Graph			
	1D-Chain	NL	FC($N_q = 20$)	FC N_q/r_{eff}
<code>ibm_brisbane</code>	0.84/0.756	0.678	0.000	16/0.009
<code>ibm_torino-v0</code>	-/0.728	0.724	0.000	15/0.006
<code>ibm_torino-v1</code>	-/0.760	0.746 f0.773	-	-
<code>ibm_fez</code>	0.87/0.776 -/f0.808	0.751 f0.782	0.020	20/0.020
<code>ibm_marrakesh</code>	0.92/0.773	f0.772	0.004	20/0.004
<code>H1-1E</code>	-/-	-	0.582	20/0.582
<code>quantinuum_H2-1</code>	-/-	-	0.555	56/0.082
<code>ionq_aria_2</code>	-/-	-	0.223	20/0.223
<code>ionq_forte</code>	-/-	-	0.269	21/0.250
<code>iqm_spark</code>	-/-	0.643	-	-
<code>iqm_garnet</code>	0.75/-	0.632	-	-
<code>rigetti_ankaa_2</code>	0.61/-	-	-	-

IV. CONCLUSIONS

In this work, we have presented a benchmarking protocol for QPUs that pushes the limits of the execution of quantum circuits in terms of the number of qubits (width) and the number of 2-qubit gate layers (depth). It is based on a fixed-parameters QAOA protocol known as LR-QAOA. We test the protocol on 19 different QPUs from 5 vendors using 3 graph topologies. The test is passed if the LR-QAOA optimization protocol can be distinguished from a random sampler. We show that we can make the distinction with a small number of samples, which is helpful for QPUs where the sampling cost is considerable. The benchmark is also stable in time; we find that the coefficient of variation in an experiment repeated 5 times in a lapse of 2 months is 1%. To the best of our knowledge, this is the largest benchmarking implementation by the number of QPUs involved, which also indicates their practicality and usefulness.

For the first topology, 1D-chain, our main test involves 100 qubits on different IBM devices. We find the best results on `ibm_fez` with a performance peak of $r = 0.776$ at $p_{eff} = 9$ involving $N_{2q} = 1,782$ CZ gates and using fractional gates $r = 0.808$ at $p_{eff} = 15$ involving $N_{2q} = 1,485$ ZZ gates. In the NL case, `ibm_fez` shows the best performance $r = 0.751$ for a 156-qubit problem at $p_{eff} = 6$ involving $N_{2q} = 2,112$ CZ gates and using fractional gates $r = 0.782$ at $p_{eff} = 15$ involving $N_{2q} = 2,640$ ZZ gates. For FC problems, `ibm_fez` shows the best performance for a 20-qubit problem with $p_{eff} = 3$ involving $N_{2q} = 1,710$ CZ gates. Our largest successful LR-QAOA implementation is a 56-qubit problem with $p = 3$ and $N_{2q} = 4,620$ ZZ gates on `quantinuum_H2-1`.

These benchmarks provide insights into the generational progress of QPUs from various vendors. IBM’s QPUs exhibit significant improvement, particularly in the transition from the Eagle to Heron generations. These improvements are not solely attributed to hardware upgrades but also to firmware improvements and the integration of fractional gates into the default gate set.

Interestingly, the latest QPU released, `ibm_marrakesh`, which follows `ibm_fez` and features half its EPLG, does not demonstrate the expected performance gains. While smaller sections of `ibm_marrakesh` deliver superior performance, the device efficiency diminishes beyond 15 qubits. This decline may come from non-local crosstalk, which seems to reduce the overall performance at larger scales.

In the case of IonQ, we observed a significant improvement in quality from `ionq_harmony` to `ionq_aria_2`, but the progression from `ionq_aria_2` to `ionq_forte` is less pronounced. The case of Quantinuum is similar to that of IonQ; both devices have comparable performance. Still, the performance of `quantinuum_H1-1` and `H2-1` is superior to that of the other QPUs. In the case of IQM, both devices show similar performance, with `iqm_garnet` being slightly better than `iqm_spark`. In the case of Rigetti, we do not have another QPU from this company to contrast results, but `Ankaa-2`’s performance is the lowest of all the QPUs tested.

Circuit depth is a key characteristic of the LR-QAOA benchmark, highlighting the challenges of implementing deep quantum circuits. Superconducting technology (IBM Eagle and Heron, IQM, or Rigetti) offers fast execution times but suffers from considerable 2-qubit gate errors. In contrast, trapped ion technology (IonQ or Quantinuum) provides acceptable 2-qubit gate error rates and full connectivity but operates slowly, incurring high shot costs. For instance, in a hypothetical 25-qubit FC problem with $p=100$ and 1,000 shots, `ionq_aria_2` would require 18,000 seconds based solely on the 2-qubit gate time, while `ibm_fez` would need 0.51 seconds. This disparity emerges from the 2-qubit gate time and the inability to execute these gates in parallel in trapped ion QPUs. This is also evident in the disparity in the number of 2-qubit gates that different vendors allow. While IBM devices support the execution of almost 1,000,000 2-qubit gates, IonQ restricts it to fewer than 650 gates, and Quantinuum fewer than 18,375. Our proposed benchmarking reveals critical bottlenecks that quantum technology must address to support algorithms with high depth and width.

There are different ways to improve the results on a given QPU; for instance, one can use dynamical decoupling [31] to reduce errors while executing the circuits. In the case of FC problems, one can also improve on fixed layout QPUs using better strategies for encoding LR-QAOA such as the ones in [32, 33] or improving in routing the qubits with techniques like [34, 35]. In the case of postprocessing the samples, we have not found any in-

dication that this technique removes errors. However, if it is found to be meaningful, the same strategy should be applied to the random sampler to make a fair comparison. Modification of the initial superposition, e.g., using warm-start [36], should not be used because it artificially improves the performance of the QPU, shifting the random limit from an equiprobable probability distribution to a biased one.

DATA AVAILABILITY

The datasets for the problems used and/or analyzed during the current study are available from the following publicly accessible repository <https://github.com/alejomonbar/LR-QAOA-QPU-Benchmarking>.

ACKNOWLEDGMENTS

J. A. Montanez-Barrera acknowledges support from the German Federal Ministry of Education and Research (BMBF), the funding program Quantum Technologies - from Basic Research to Market, project QSolid (Grant No. 13N16149). D. E. Bernal Neira acknowledges the support of the startup grant of the Davidson School of Chemical Engineering at Purdue University. We acknowledge the support of the Quantum Collaborative for their support and access to IBM Quantum Resources. The views expressed are those of the authors and do not reflect the official policy or position of IBM or the IBM Quantum team.

This research used resources of the Oak Ridge Leadership Computing Facility for the experiments on `quantinuum.H2`, which is a DOE Office of Science User Facility supported under Contract DE-AC05-00OR22725.

-
- [1] J. A. Montanez-Barrera and K. Michielsen, Towards a universal qaoa protocol: Evidence of a scaling advantage in solving some combinatorial optimization problems (2024), arXiv:2405.09169 [quant-ph].
- [2] A. W. Cross, L. S. Bishop, S. Sheldon, P. D. Nation, and J. M. Gambetta, Validating quantum computers using randomized model circuits, *Phys. Rev. A* **100**, 032328 (2019).
- [3] P. Jurcevic, D. Zajac, J. Stehlik, I. Lauer, and R. Mandelbaum, Ibm quantum has achieved its highest quantum volume yet (2022), accessed: 2024-07-05.
- [4] S. A. Moses, C. H. Baldwin, M. S. Allman, R. Ancona, L. Ascarrunz, C. Barnes, J. Bartolotta, B. Bjork, P. Blanchard, M. Bohn, J. G. Bohnet, N. C. Brown, N. Q. Burdick, W. C. Burton, S. L. Campbell, J. P. Campora, C. Carron, J. Chambers, J. W. Chan, Y. H. Chen, A. Chernoguzov, E. Chertkov, J. Colina, J. P. Curtis, R. Daniel, M. DeCross, D. Deen, C. Delaney, J. M. Dreiling, C. T. Ertsgaard, J. Esposito, B. Estey, M. Fabrikant, C. Figgatt, C. Foltz, M. Foss-Feig, D. Francois, J. P. Gaebler, T. M. Gatterman, C. N. Gilbreth, J. Giles, E. Glynn, A. Hall, A. M. Hankin, A. Hansen, D. Hayes, B. Higashi, I. M. Hoffman, B. Horning, J. J. Hout, R. Jacobs, J. Johansen, L. Jones, J. Karcz, T. Klein, P. Lauria, P. Lee, D. Liefer, S. T. Lu, D. Lucchetti, C. Lytle, A. Malm, M. Matheny, B. Mathewson, K. Mayer, D. B. Miller, M. Mills, B. Neyenhuis, L. Nugent, S. Olson, J. Parks, G. N. Price, Z. Price, M. Pugh, A. Ransford, A. P. Reed, C. Roman, M. Rowe, C. Ryan-Anderson, S. Sanders, J. Sedlacek, P. Shevchuk, P. Siegfried, T. Skripka, B. Spaun, R. T. Sprenkle, R. P. Stutz, M. Swallows, R. I. Tobey, A. Tran, T. Tran, E. Vogt, C. Volin, J. Walker, A. M. Zolot, and J. M. Pino, A race-track trapped-ion quantum processor, *Phys. Rev. X* **13**, 041052 (2023).
- [5] AQT, State of quantum computing in europe: Aqt pushing performance with a quantum volume of 128 (2023), accessed: 2024-07-05.
- [6] I. Q. Computers, Iqm garnet 20q whitepaper 2024 (2024), accessed: 2024-07-05.
- [7] Quantinuum, Quantinuum hardware - quantum volume (2023), accessed: 2024-10-15.
- [8] J. Emerson, R. Alicki, and K. Życzkowski, Scalable noise estimation with random unitary operators, *Journal of Optics B: Quantum and Semiclassical Optics* **7**, S347–S352 (2005).
- [9] T. J. Proctor, A. Carignan-Dugas, K. Rudinger, E. Nielsen, R. Blume-Kohout, and K. Young, Direct randomized benchmarking for multiqubit devices, *Physical Review Letters* **123**, 10.1103/physrevlett.123.030503 (2019).
- [10] T. Proctor, S. Seritan, K. Rudinger, E. Nielsen, R. Blume-Kohout, and K. Young, Scalable randomized benchmarking of quantum computers using mirror circuits, *Physical Review Letters* **129**, 10.1103/physrevlett.129.150502 (2022).
- [11] S. Boixo, S. V. Isakov, V. N. Smelyanskiy, R. Babush, N. Ding, Z. Jiang, M. J. Bremner, J. M. Martinis, and H. Neven, Characterizing quantum supremacy in near-term devices, *Nature Physics* **14**, 595 (2018), arXiv:1608.00263.
- [12] J.-S. Chen, E. Nielsen, M. Ebert, V. Inlek, K. Wright, V. Chaplin, A. Maksymov, E. Páez, A. Poudel, P. Maunz, and J. Gamble, Benchmarking a trapped-ion quantum computer with 29 algorithmic qubits, *Quantum* (2023), arXiv:2308.05071.
- [13] D. C. McKay, I. Hincks, E. J. Pritchett, M. Carroll, L. C. G. Govia, and S. T. Merkel, Benchmarking quantum processor performance at scale (2023), arXiv:2311.05933 [quant-ph].
- [14] T. Lubinski, S. Johri, P. Varosy, J. Coleman, L. Zhao, J. Necaie, C. H. Baldwin, K. Mayer, and T. Proctor, Application-oriented performance benchmarks for quantum computing, *IEEE Transactions on Quantum Engineering* **4**, 1–32 (2023).
- [15] J.-S. Chen, E. Nielsen, M. Ebert, V. Inlek, K. Wright, V. Chaplin, A. Maksymov, E. Páez, A. Poudel, P. Maunz, and J. Gamble, Benchmarking a trapped-ion quantum computer with 29 algorithmic qubits (2023), arXiv:2308.05071 [quant-ph].
- [16] T. Lubinski, C. Coffrin, C. McGeoch, P. Sathe, J. Apanavicius, and D. E. B. Neira, Optimization applications as quantum performance benchmarks (2024), arXiv:2302.02278 [quant-ph].
- [17] R. Blume-Kohout and K. C. Young, A volumetric framework for quantum computer benchmarks, *Quantum* **4**, 362 (2020).
- [18] M. Amico, H. Zhang, P. Jurcevic, L. S. Bishop, P. Nation, A. Wack, and D. C. McKay, Defining standard strategies for quantum benchmarks (2023), arXiv:2303.02108 [quant-ph].
- [19] IBM, Introducing the heavy-hex lattice (2020), [Accessed: 01-Jul-2024].
- [20] E. Farhi, J. Goldstone, and S. Gutmann, A quantum approximate optimization algorithm (2014), arXiv:1411.4028 [quant-ph].
- [21] R. M. Karp, R. E. Miller, and J. W. Thatcher, Reducibility among combinatorial problems, *Journal of Symbolic Logic* **40** (1975).
- [22] F. Barahona, On the computational complexity of ising spin glass models, *Journal of Physics A: Mathematical and General* **15**, 3241 (1982).
- [23] E. Farhi, J. Goldstone, S. Gutmann, and M. Sipser, Quantum computation by adiabatic evolution, arXiv preprint quant-ph/0001106 (2000).
- [24] I. Quantum, Ibm quantum services and resources, <https://quantum.ibm.com/services/resources> (2024), accessed: 2024-07-29.
- [25] Microsoft, Ionq aria quantum computer, <https://learn.microsoft.com/en-us/azure/quantum/provider-ionq#ionq-aria-quantum-computer> (2024), accessed: 2024-07-29.
- [26] Quantinuum, H1 quantum computer, <https://www.quantinuum.com/hardware/h1> (2024), accessed: 2024-07-29.
- [27] Quantinuum, H2 quantum computer, <https://www.quantinuum.com/hardware/h2> (2024), accessed: 2024-07-29.
- [28] AWS, Amazon braket devices - ankaa-2, <https://aws.amazon.com/> (2024), accessed: 2024-08-29.
- [29] I. Quantum, Fractional gates: A breakthrough in quantum computing, <https://www.ibm.com/quantum/blog/>

- `fractional-gates`, accessed: 2024-12-19.
- [30] H. De Raedt, F. Jin, D. Willsch, M. Willsch, N. Yoshioka, N. Ito, S. Yuan, and K. Michielsen, Massively parallel quantum computer simulator, eleven years later, *Computer Physics Communications* **237**, 47 (2019).
 - [31] N. Ezzell, B. Pokharel, L. Tewala, G. Quiroz, and D. A. Lidar, Dynamical decoupling for superconducting qubits: A performance survey, *Physical Review Applied* **20**, 10.1103/physrevapplied.20.064027 (2023).
 - [32] Y. Ji, X. Chen, I. Polian, and Y. Ban, Algorithm-oriented qubit mapping for variational quantum algorithms (2024), arXiv:2310.09826 [quant-ph].
 - [33] B. Klaver, S. Rombouts, M. Fellner, A. Messinger, K. Ender, K. Ludwig, and W. Lechner, Swap-less implementation of quantum algorithms (2024), arXiv:2408.10907 [quant-ph].
 - [34] P. D. Nation and M. Treinish, Suppressing quantum circuit errors due to system variability, *PRX Quantum* **4**, 10.1103/prxquantum.4.010327 (2023).
 - [35] J. A. Montañez-Barrera, G. P. Beretta, K. Michielsen, and M. R. von Spakovsky, A zero-entropy classical shadow reconstruction of density state operators (2024), arXiv:2408.17317 [quant-ph].
 - [36] D. J. Egger, J. Mareček, and S. Woerner, Warm-starting quantum optimization, *Quantum* **5**, 479 (2021).
 - [37] C. Bliiek, P. Bonami, and A. Lodi, Solving mixed-integer quadratic programming problems with ibm-cplex : a progress report (2014).
 - [38] V. Kremenetski, T. Hogg, S. Hadfield, S. J. Cotton, and N. M. Tubman, Quantum alternating operator ansatz (qaoa) phase diagrams and applications for quantum chemistry (2021), arXiv:2108.13056 [quant-ph].
 - [39] Y. Hirata, An efficient method to convert arbitrary quantum circuits to ones on a Linear Nearest Neighbor architecture, 2009 Third International Conference on Quantum, Nano and Micro Technologies , 26 (2009).
 - [40] Y. Jin, J. Luo, L. Fong, Y. Chen, A. B. Hayes, C. Zhang, F. Hua, and E. Z. Zhang, A Structured Method for Compiling and Optimizing QAOA Circuits in Quantum Computing, arXiv <https://doi.org/10.48550/arXiv.2112.06143> (2021), arXiv:arXiv:2112.06143v4.

Appendix A: Supplementary Material

1. MaxCut

The WMC problem involves determining the partition of the vertices in an undirected graph so that the total weight of the edges between the two sets is maximized. This problem has the desired properties that can be adapted to different graphs and does not contain constraints. For an undirected graph $G = (V, E)$, the Hamiltonian is formulated as

$$H_C = \sum_{(i,j) \in E} w_{ij} \sigma_i \sigma_j, \quad (\text{A1})$$

where w_{ij} represents the weight of the edge between vertices i and j . The goal is to maximize the sum of edge weights over all edges in the cut, which corresponds to finding the ground state of Eq. A1. When sampling, the binary variables associated with each qubit x_i take values of 0 or 1, indicating the membership of vertices in one of the 2 sets. If x_i and x_j are different, the edge weight w_{ij} contributes to the objective function.

We use the approximation ratio as a metric of the performance of the MaxCut and its variations. The approximation ratio is given by

$$r = \frac{\sum_{i=1}^n C(x_i)/n}{C(x^*)}, \quad (\text{A2})$$

$$C(x) = \sum_{k,l>k}^{N_q} w_{kl}(x_k + x_l - 2x_k x_l), \quad (\text{A3})$$

where n is the number of samples, x_i the i th bitstring obtained from LR-QAOA, and $C(x)$ is the cost function of WMC, x^* is the optimal bitstring, $C(x^*)$ is the maximum cut, w_{kl} is the weight of the edge between nodes k and l , and x_k is the k th position of the x bitstring. In our benchmarks, optimal solution x^* can be efficiently found using classical solvers, e.g., CPLEX [37] for thousands of variables. In the case of larger size problems where optimality cannot be guaranteed, the best-known solution can be considered instead of x^* . This methodology ensures unlimited scalability.

2. Random sampling limit

To certify if the result of a QPU is still meaningful, we compare the approximation ratio for the LR-QAOA WMC problem given by the samples of the QPU to those coming from a random sampler. Because noise affects the QPU, three stages of the sampling results of the QPU can be distinguished: the first stage is when the result is still meaningful, i.e., the approximation ratio is above the interval of confidence of a random sampler. The second stage is where the results are similar to those from a random sampler, meaning that the QPU result is fully mixed. The third stage is when other QPU phenomena give results that are below the random limit confidence interval. This stage is observed when a large number of layers is applied, for instance, the results of the 5-qubit NL IQM Spark in Fig. 3-(b) at $p=100$, which requires 800 2-qubit gates or the 100-qubit `ibm_torino` FC problem which requires 297,000 2-qubit gates for $p = 20$. The result of the 100-qubit `ibm_torino` experiment at $p = 20$ is shown in Fig. 6.

Figure 5 shows three cases of the FC benchmarking from the sampling standpoint and its comparison with the random sampler. Figs. 5(a)-(b) shows two cases for `quantinuum_H2-1`; in the first case, 50 samples are used, while in the second, only 7 samples are used. As the number of samples decreases, the shaded region of the confidence interval expands, but even in that case, distinguishing between samples from a random sampler and those produced by the LR-QAOA is possible. As sampling costs are relatively high for some quantum technology, meaningful results are desired even with a small number of samples. In the case of `ibm_fez`, Fig. 5(c), 1000 samples are used because the cost of sampling in this technology is low. The interval of confidence of random sampling, in this case, is narrow.

To certify if a given distribution of LR-QAOA samples is doing an optimization and therefore above the random limit, we use the effective approximation ratio r_{eff} given by

$$r_{\text{eff}} = \frac{r_{\text{max}} - r_{\text{rand}}}{1 - r_{\text{rand}}}, \quad (\text{A4})$$

where r_{max} is the WMC LR-QAOA mean approximation ratio at p_{eff} , r_{rand} is the mean approximation ratio of the random samples on the WMC problem plus 3 standard deviations of the mean approximation ratio over the different

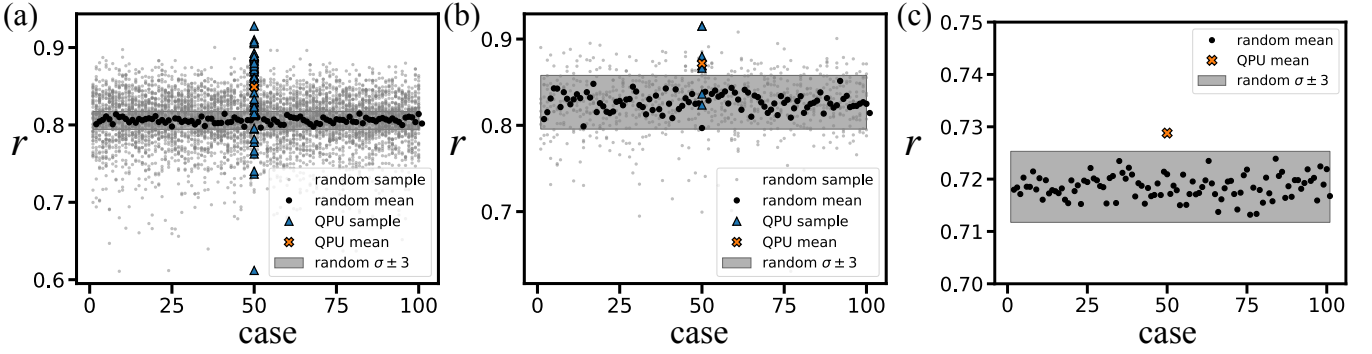


FIG. 5. LR-QAOA WMC approximation ratios of QPUs' samples compared to a random sampler. The x-axis represents the random sampler case index. The QPU's result is arbitrarily shown in the middle of the plot. (a) H2-1 50-qubit, 50 samples, and $p = 4$, (b) 56-qubit, 7 samples, and $p = 3$, (c) `ibm_fez` 20-qubit, 1000 samples, and $p = 3$. Dots correspond to a single random bitstring approximation ratio, the dark circle is the mean value over the random samples for each case, the triangles are individual samples of the QPU, and the X marker is the mean value of the QPU's samples, the shaded region corresponds to the confidence interval of 3 standard deviations of the mean value of all the dark circles. In plot (c) the samples are not shown for visualization purposes.

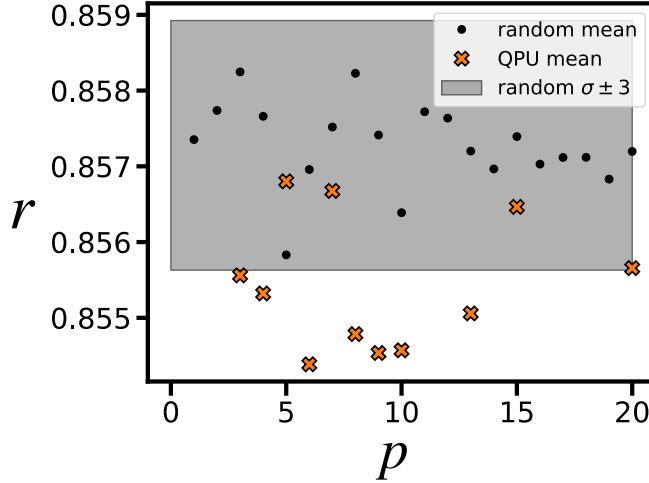


FIG. 6. LR-QAOA WMC approximation ratios of `ibm_torino` for a FC problem with 100 qubits from $p=3$ to $p=20$. 20 random cases are shown with the same characteristics as in Fig.5.

subset of samples, for instance, if the experiment has 50 samples, the mean value is collected over 100 subsets of 50 samples, for each subset the mean value is calculated. If $r_{\text{eff}} > 0$, it means with 99.73% confidence that the LR-QAOA is doing some optimization.

3. Experimental $\Delta_{\gamma,\beta}$ used

For the 1D-Chain and NL problems, we use $\Delta_{\beta,\gamma} = 1$. For the FC graph, different values are chosen, for $N_q \leq 15$, a value of $\Delta_{\gamma,\beta} = 0.63$ independent of the QPU. For $N_q > 15$ values are summarized in Table III. The difference in values does not reflect any parameter tuning; instead, they are chosen following a characteristic found in [1] Sec.III-B that as N_q grows $\Delta_{\beta,\gamma}$ must decrease to keep performance. Certainly, one can find a function of $\Delta_{\gamma,\beta}(N_q)$ for a better estimation of the parameters, or one can scan the $\Delta_{\gamma,\beta}$ that gives the best performance, as it is shown in Fig. 8-(a) and Fig. 9-(b).

TABLE III. Backends $\Delta_{\gamma,\beta}$ used.

	Backend															
	ibm_fez(marrakesh)	ibm_torino		ibm_brisbane			H1-1E		H2-1E			H2-1		ionq_aria_2		qasm_simulator
N_q	> 15	17	20	16	17	20	20	25	30	40	50	56	17	20	20	25
$\Delta_{\beta,\gamma}$	0.63	0.4	0.3	0.5	0.4	0.3	0.3	0.5	0.4	0.2	0.2	0.2	0.63	0.3	0.3	0.4

4. Performance diagram

The performance diagram, proposed in [38], helps to identify the set of $\Delta_{\gamma,\beta}$ that fit best on LR-QAOA for a given problem. Fig. 7(a) shows the ideal case, i.e., where there is no noise in the LR-QAOA evolution. This evolution is characterized by a continuous improvement in the approximation ratio as the number of LR-QAOA layers is increased. On the other hand, Fig. 7(b) shows the performance diagram on a real QPU. In this case, noise affects the evolution, impacting the performance of the LR-QAOA algorithm. Therefore, when dealing with a real QPU, there is an optimal p to get the best performance. In this case, $p = 3$ to $p = 8$ have points of similar performance, which makes it optimal to select the minimum number of p layers as they will require less time and resources.

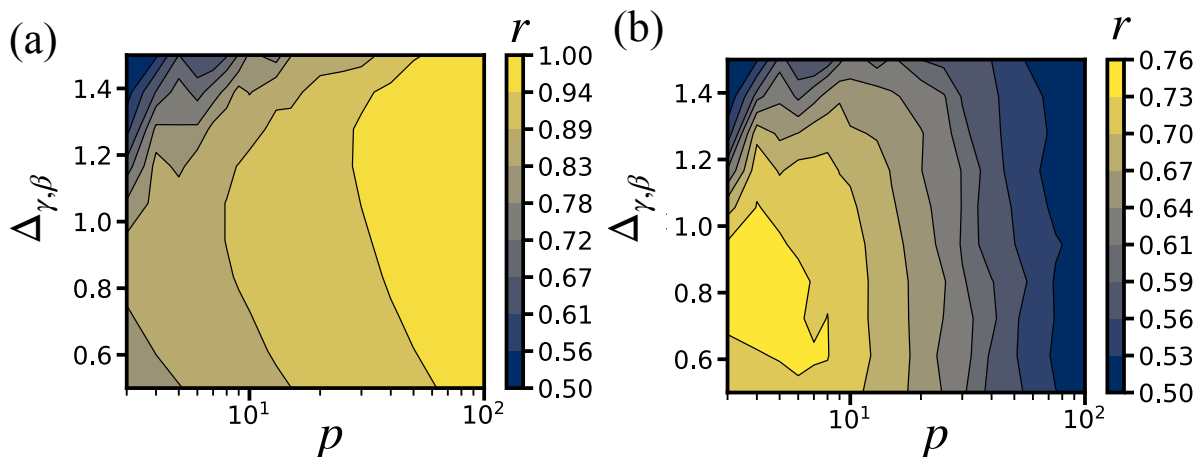


FIG. 7. Performance diagram of a 30-qubit 1D-Chain WMC using LR-QAOA with $p=3$ to 100 on (a) state vector simulator (b) `ibm_brisbane`. The color bar represents the approximation ratio for a given p and $\Delta_{\gamma,\beta}$.

5. 1D-chain Benchmarking

Results of the 1D-chain are thought to give a meaningful diagnostic of the qubits in the largest chain of qubits on a given QPU. The motivation behind this is that an FC interaction on a fixed layout device can be created using a 1D-chain with depth growing $O(N_q)$ using the SWAP strategy presented in Sec. A 7.

In Fig. 8, we show the results of the LR-QAOA 1D-Chain experiments on different IBM QPUs, IQM Garnet, and Rigetti Ankaa. Fig. 8(a) shows the performance diagram of the approximation ratio for a given $\Delta_{\gamma,\beta}$ and p on `ibm_brisbane` for a 100-qubit WMC random problem. This map is used to select a good set of $\Delta_{\gamma,\beta} = 1$ for the remaining 1D-chain experiments.

Fig. 8(b) shows a 5-qubit 1D-Chain WMC problem running on different sections of `ibm_brisbane`. The case highlighted in black corresponds to the section with the best performance in terms of the maximum approximation ratio. Figure 8(c) shows the corresponding approximation ratio at each section of the device. In the case of `ibm_brisbane` with 109 qubits in its main diagonal, 21 sections are available to run this test, the region with the best approximation ratio is presented by the arrow. The same methodology is used with the other devices for the 1D-chain problems and the FC problems.

Fig. 8(d) shows the approximation ratio versus the number of LR-QAOA layers for different problem sizes. The maximum approximation ratio reached seems proportional to the number of qubits but there is a small gap between the 30-qubit and 100-qubit problems. This is explained by the approximation ratio of LR-QAOA, which gives an estimate of the average performance of the qubits involved.

Fig. 8(e) shows the behavior of the approximation ratio of `ibm_brisbane` for a 100-qubit problem executed during different days with the maximum elapsed time of 2 months since the first experiment took place. The standard deviation in the peak of the approximation ratio is $\sigma = \pm 0.007$, and the mean value at the peak $\mu = 0.750$, this means a coefficient of variation $\sigma/\mu = 1\%$ which shows that the experiment is stable and consistent, an ideal characteristic when benchmarking a device.

Fig. 8(f) presents the results of a 60-qubit 1D-chain WMC problem using three devices, compared with a Matrix Product State (MPS) simulator. The data shows continuous improvements in device quality, with `ibm_brisbane` being the oldest, followed by `ibm_torino-v0`, and `ibm_torino-v1`, which features updated firmware for `ibm_torino`. Although the MPS simulator approximates the real dynamics, it provides a reliable representation of the true evolution of LR-QAOA due to the graph's simple connectivity.

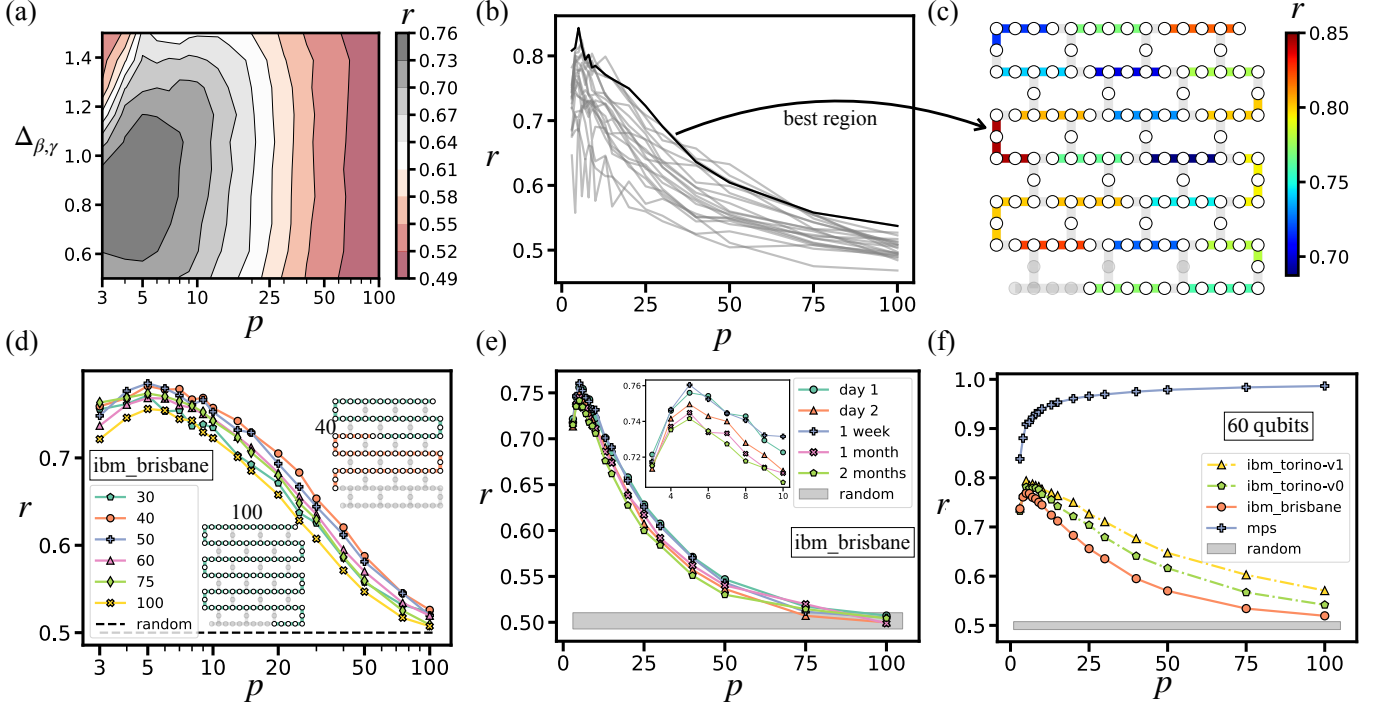


FIG. 8. 1D-chain WMC using LR-QAOA with $p=3$ to 100 and problem sizes between 19 and 100 qubits on IBM, IQM, and Rigetti devices. (a) Performance diagram of the 100-qubit problem on `ibm_brisbane`. The shaded region (random) indicates the limit of a random sample with an interval of confidence of $\pm 3\sigma$ in the three plots represents the random limit. (b) 5-qubit problem different sections results on `ibm_brisbane`, the result highlighted in black is the result of the best section of the QPU. (c) `ibm_brisbane` layout with the results of the 5-qubit problem of (c) and the corresponding section of the device. The edge color represents the approximation ratio in the section. (d) Problem on `ibm_brisbane` from problem size ranging from 30 to 100 qubits. The inset shows the selected qubits for the 40-qubit and 100-qubit cases. In the 40-qubit case, the problem is repeated 2 times in the devices (green and orange chains); the results shown are from the section with the best approximation ratio. (e) Approximation ratio versus p for a 100-qubit problem, repetition during different days with day 1 the starting day. (f) Approximation ratio versus p of a 60-qubit problem solved using `ibm_torino` and `ibm_brisbane` and comparing it with the simulation using MPS.

6. Native Layout Benchmarking

Figure. 9 shows the solutions of native graph problems involving the full set of qubits and 2-qubit gates for different QPUs. Fig. 9 (a) shows the layout of a 133-qubit Heron r1 device (`ibm_torino`). In this device, to implement the LR-QAOA protocol, three sublayers of 2-qubit gates are required, in these sublayers, a similar number of 2-qubit gates are run in parallel. Fig. 9 (b) shows the approximation ratio phase diagram for the LR-QAOA native graph experiment on `ibm_torino`. This diagram indicates where the optimal $\Delta_{\beta,\gamma}$ and p are for a given device. Note that in the ideal case, the r must approach 1 in the case of an ideal device, similar to what is shown in Fig. 7(a). We choose $\Delta_{\beta,\gamma} = 1$ for subsequent experiments.

Figure 9 (c) shows the solution of the native graph problem on different IBM Eagle QPUs. Results show that *ibm.kyiv*, the device with the lowest EPLG, gives the best approximation ratio. However, the quality of the solutions from the other devices does not fully agree with the EPLG at the moment of the experiment. All the devices seem to have the same $p_{eff} = 4$.

Figure 9 (d) shows r versus the number of LR-QAOA layers for different random problems on *ibm.fez*. The different curves represent different seeds for the weights of the WMC. Note there is a slight variation in the quality of the solutions for the different seeds with a standard deviation at the maximum approximation ratio of ± 0.005 . This is a good characteristic for benchmarking native graph problems because no specific problem needs to be implemented but only the choice of the random values set must be fixed. In the case of the NL problems presented the values are 0.1, 0.2, 0.3, 0.5, and 1.0.

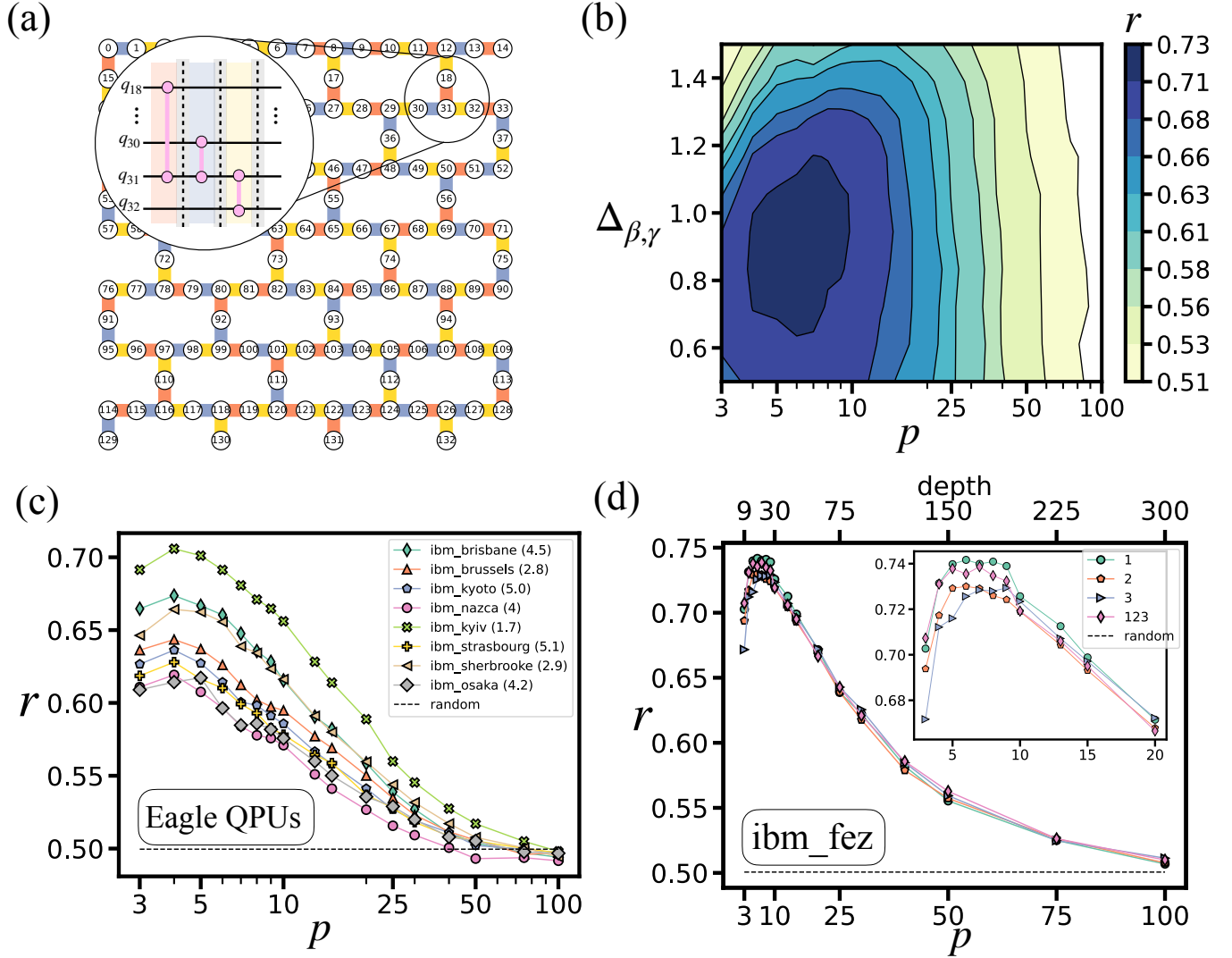


FIG. 9. Layout-based benchmarking using LR-QAOA for WMC problems with 20, 127, 133, and 156 qubits on *iqm.garnet*, *ibm_brisbane*, *ibm_torino*, and *ibm_fez*, respectively. (a) *ibm_torino* layout. The colors refer to the two-qubit gates executed at the same time-step of each layer of LR-QAOA. The inset shows the 2-qubit depth 3 needed to execute the two-qubit gates 18-31, 30-31, and 31-32. (b) Performance diagram of the native graph experiment on *ibm_torino*. (c)-(d) Shows the approximation ratio versus LR-QAOA layers of the WMC. The dashed line in these plots represents the random limit. (c) Comparison of different IBM Eagle devices. The value in parentheses next to each device is the EPLG. (d) Results using different seeds of the random weights on *ibm_fez*.

7. SWAP strategy

In the case of FC graph problems for fixed layout QPUs, we use a strategy of converting a 1D chain onto an FC using a linear swap network [39, 40]. The linear swap network strategy is shown in Fig.10-(a). Here, the y-axis represents the physical qubits and the x-axis denotes the timestep. The logical qubits are depicted as circles, each with a distinct color. At each timestep, the logical qubit is in a different physical qubit position. The dotted lines crossing each other indicate the interchange of two logical qubits. In terms of the quantum circuit, this interchange is a SWAP gate, as the one shown inside the red oval in Fig.10-(b).

The swap network strategy requires $O(N_q(N_q - 1)/2)$ SWAP gates and increases the depth of the circuit N_q times the time required for a SWAP gate for each layer p of the QAOA algorithm. In a QPU utilizing a default gate set with the CNOT gate, a SWAP gate can be decomposed into three CNOT gates, while the RZZ gate can be decomposed into two CNOT gates with an intermediate RZ gate, as illustrated in Fig.10-(c). Combining the $RZZ(2\gamma Q_{ij})$ gate and the SWAP gate removes two CNOT gates. Therefore, for an FC COP involving N_q qubits and using p QAOA layers, the number of CNOTs required is $3N_q(N_q - 1)/2$.

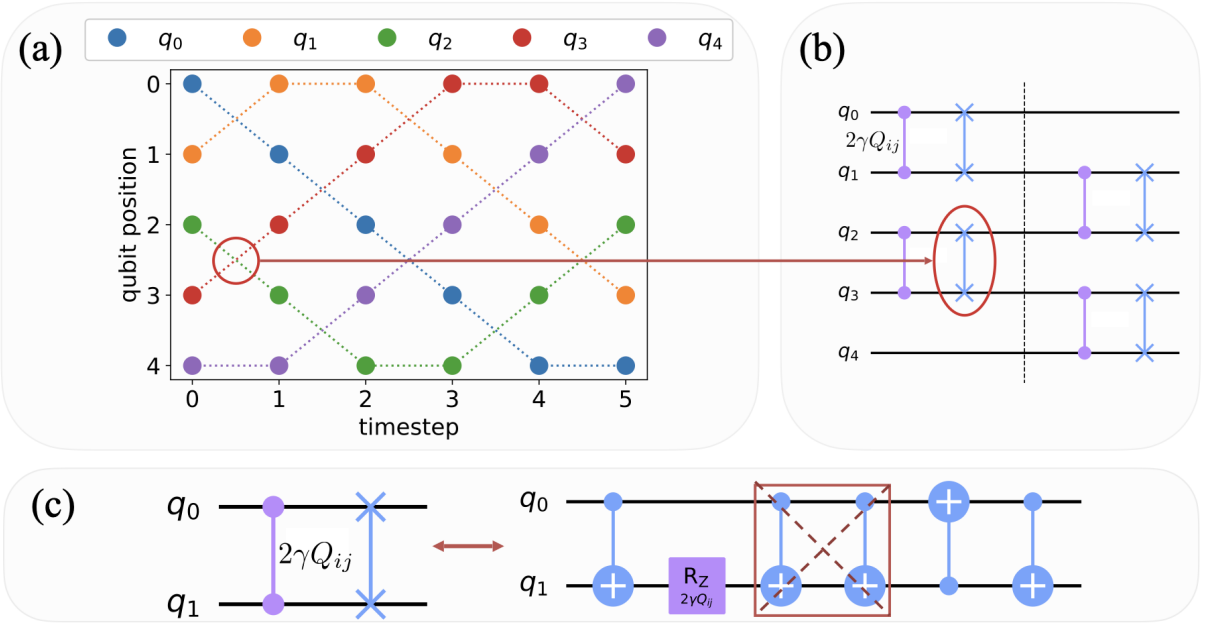


FIG. 10. (a) linear SWAP network strategy, the colored circles represent the logical qubits, and the y-axis represents the physical qubit position (b) circuit representation of the linear SWAP network strategy combined with the two-qubit terms in the QUBO (c) circuit reduction SWAP and RZZ gate.

8. Correlation in LR-QAOA

In Fig. 11, we show how the correlation between variables in a 10-qubit FC problem looks like on different QPUs at two different numbers of layers p . The correlation $|C_{ij}|$ is given by

$$|C_{ij}| = \left| \sum_{n=0}^N s_i^n s_j^n \right| \quad (\text{A5})$$

where n is a given samples, N is the total number of samples, $s_i^n \in \{0, 1\}$ is spin i in sample n , and N_q is the total number of qubits. In Fig.11(a), `qasm_simulator` refers to a noiseless simulation of the true evolution of LR-QAOA. From the 3 QPUs analyzed, the H1-E is the one that resembles better the LR-QAOA noiseless evolution, with an improvement from $p=3$ to $p=9$ followed by `ionq_aria_2` which shows a larger correlation at $p=3$ but low at $p=9$, and then `ibm_fez` that shows some characteristics of the ideal correlation at $p=3$ but almost vanished correlations at $p=9$. Fig. 11-(b) shows the same experiments in terms of the approximation ratio vs. the number of LR-QAOA layers.

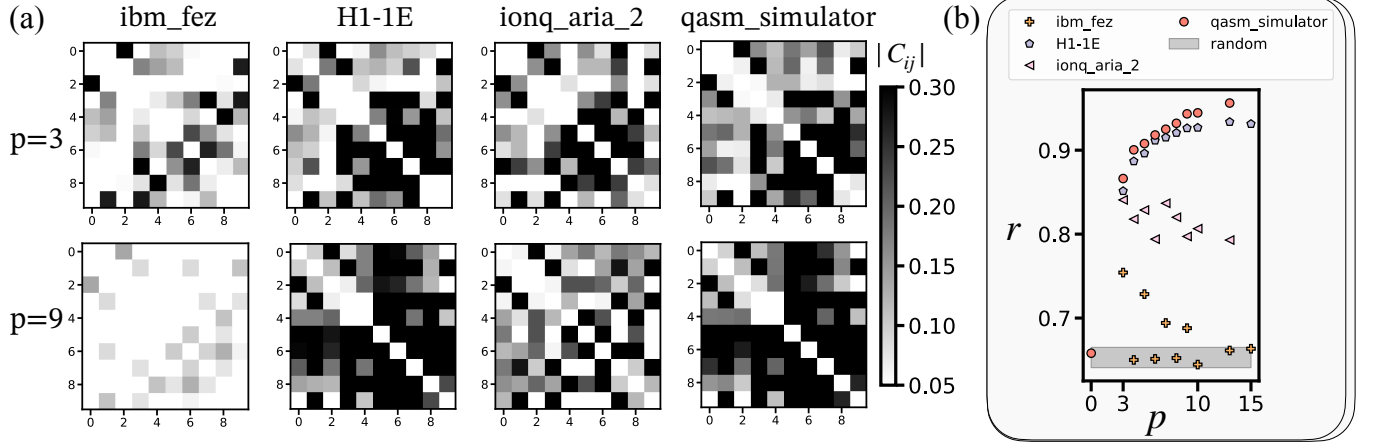


FIG. 11. FC 10-qubit WMC results using LR-QAOA on different QPUs. (a) upper row correlation matrix at $p = 3$ and lower row at $p = 9$. (b) Approximation ratio vs. number of LR-QAOA layers.

9. Speed of execution

In Fig.12, we show the execution time expected by the different QPUs. It is important to mention the time because it can become a bottleneck in the successful implementation of quantum algorithms. So, special care must be taken by quantum vendors to improve quantum hardware in this direction, too. For instance, running a 50-qubit with $p = 50$ only counting the 2-qubit gates time takes $510 \mu\text{s}$ using `ibm_fez` and 36.75 s using `ionq_aria_2`. In the case of a 100-qubit problem, it would take $2040 \mu\text{s}$ and 297 s , and a 200-qubit problem $8116 \mu\text{s}$ and 2388 s , respectively.

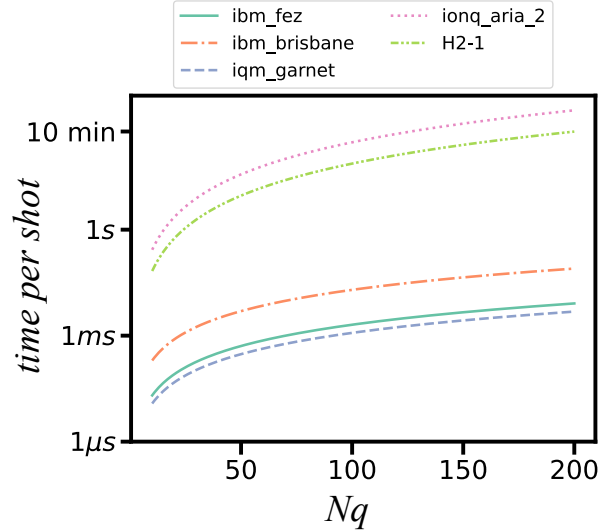


FIG. 12. Projection of the time required by different QPUs to run one instance of an FC LR-QAOA problem using $p = N_q$ layers. The `quantinuum_H2-1` line is an estimate using the 2-qubit time of Aria-1 because no information about the 2-qubit time is provided for this device.